REPORT DOCUMENTATION PAGE

1. REPORT DATE (DD-MM-YYYY)	2. REPORT TYPE	3. DATES COVERED (From - To)
1-03-2000	Journal Article	1999

4. TITLE AND SUBTITLE

Change in microscopic tunneling on a macroscopic time scale: Current surge model

5a. CONTRACT NUMBER

5b. GRANT NUMBER

5c. PROGRAM ELEMENT NUMBER
62601F

6. AUTHOR(S)

Danhong Huang, D.A. Cardimona, and Anjali Singh

5d. PROJECT NUMBER
4846

5e. TASK NUMBER
CR

5f. WORK UNIT NUMBER
C1

7. PERFORMING ORGANIZATION NAME(S) AND ADDRESS(ES)

Air Force Research Laboratory
Space Vehicles Directorate
3550 Aberdeen Ave. SE
Kirtland AFB, NM 87117-5776

8. PERFORMING ORGANIZATION REPORT NUMBER

9. SPONSORING / MONITORING AGENCY NAME(S) AND ADDRESS(ES)

10. SPONSOR/MONITOR'S ACRONYM(S)

11. SPONSOR/MONITOR'S REPORT NUMBER(S)

12. DISTRIBUTION / AVAILABILITY STATEMENT

Approved for Public Release; Distribution is Unlimited.

20050201 021

13. SUPPLEMENTARY NOTES

14. ABSTRACT

The current surge model is proposed to calculate the tunneling current in multiple quantum well structures in the presence of a slow time-dependent electric field. The microscopic origin of a zero-bias residual current observed and reported previously [A. Singh and D. A. Cardimona, Opt. Eng. (Bellingham) **38**, 1424 (1999)] is explored. The mystery of the observation of a microscopic tunneling change on a macroscopic time scale is uncovered, and an involvement of a very slow physical process is shown. Some new features, such as a current "ripple," a current instability, a current hysteresis, and a current "arch," are predicted and confirmed experimentally.

15. SUBJECT TERMS

hysteresis, quantum wells, microscopic,

16. SECURITY CLASSIFICATION OF:

a. REPORT	b. ABSTRACT	c. THIS PAGE	17. LIMITATION OF ABSTRACT	18. NUMBER OF PAGES	19a. NAME OF RESPONSIBLE PERSON
Unclassified	Unclassified	Unclassified	Unlimited	5	Mr. David Cardimona

19a. NAME OF RESPONSIBLE PERSON
Mr. David Cardimona

19b. TELEPHONE NUMBER (include area code)
(505) 846-5807

Change of microscopic tunneling on a macroscopic time scale: Current surge model

Danhong Huang,[a] Anjali Singh, and D. A. Cardimona

Air Force Research Laboratory (AFRL/VSSS), 3550 Aberdeen Avenue S.E., Building 426, Kirtland Air Force Base, New Mexico 87117

The current surge model is proposed to calculate the tunneling current in multiple quantum well structures in the presence of a slow time-dependent electric field. The microscopic origin of a zero-bias residual current observed and reported previously [A. Singh and D. A. Cardimona, Opt. Eng. (Bellingham) **38**, 1424 (1999)] is explored. The mystery of the observation of a microscopic tunneling change on a macroscopic time scale is uncovered, and an involvement of a very slow physical process is shown. Some new features, such as a current "ripple," a current instability, a current hysteresis, and a current "arch," are predicted and confirmed experimentally. © 2000 American Institute of Physics. [S0021-8979(00)01205-6]

I. INTRODUCTION

In a recent article,[1] the two authors found, experimentally, a residual tunneling current in multiple quantum well (MQW) structures when a time-dependent bias voltage, which steps from −5 to 5 V in steps lasting from 5 to 60 s, sweeps through zero. A circuit model, which introduced an important leakage resistance in series with a capacitance, was devised to explain this phenomena, and a satisfactory numerical simulation was obtained. This simulation indicates that a physical process with a very large time constant is involved. However, the microscopic origin of this observation remained a mystery. It is known that the QW capacitance in MQW structures is on the order of $C_{QW} \sim 10^{-10}$ F, leading to a negligible charging energy $e^2/2C_{QW}$ when an electron is added to a QW. This is in contrast to the Coulomb blockade effect[2] observed in quantum dots which results in a much smaller capacitance compared to C_{QW}. However, the resistance of the sequential electron tunneling (SET) in the MQWs can reach as high as $R \sim 10^{11}$ Ω at low bias voltages and temperatures. Consequently, the macroscopic charging/discharging time (MCDT) in the MQWs is in the range of $RC_{QW} \sim 10$ s, which is much greater than the microscopic resonant electron tunneling (RET) time $\tau_t < 1$ ps in a double QW.[3] The question that arises is: *Why can we observe a change of the microscopic tunneling on a macroscopic charging/discharging time scale?* In order to resolve this issue and to get a complete understanding of the microscopic origin of the previously observed zero-bias residual tunneling current (ZBRTC), as well as to provide in-depth theoretical explanations for some recently observed phenomena which we describe as a current "ripple," a current instability, a current hysteresis, and a current "arch," we introduce a current surge model (CSM). Our proposed model successfully reproduces and explains all of the observations.

It is obvious that RET can occur only when the barrier between the adjacent QWs is thin. If the barrier is very thick, the phase of the wave function will be lost as an electron tunnels from one barrier to another. As a result, only SET exists for thick barriers. When the electric field $\mathcal{E}_b(t)$ is fixed at zero, the SET current $I_a[\mathcal{E}_b(t)]$ is also zero. However, $I_a[\mathcal{E}_b(t)]$ will be finite when $\mathcal{E}_b(t)$ is nonzero and varies extremely slowly with time. In this case, electrons in the MQWs are said to be in a steady state, and $I_a[\mathcal{E}_b(t)]$ is driven by $\mathcal{E}_b(t)$ only through nonlinear current–voltage characteristics. If $\mathcal{E}_b(t)$ is switched suddenly from one value to another at a particular time, $I_a[\mathcal{E}_b(t)]$ will deviate from the previous steady state and slowly relax into a new steady state. We would like to determine the characteristic time for $I_a[\mathcal{E}_b(t)]$ to switch from the old to the new steady state. Of course, within the adiabatic model, $I_a[\mathcal{E}_b(t)]$ can follow $\mathcal{E}_b(t)$ instantaneously, switching from one steady state to another with no time delay. Therefore, in order to find the true switching time, we have developed the CSM that moves well beyond the adiabatic limit.

The organization of this article is as follows. In Sec. II, we present our current surge model beyond the adiabatic limit for deriving the dynamical equation of the nonadiabatic field in the system. Numerical results and discussions are presented in Sec. III for the total electron sequential tunneling currents under either a step-like or a sinusoidal time-dependent electric field. Experimental results and comparisons are shown in Sec. IV for the total electron sequential tunneling current under a sinusoidal time-dependent bias voltage. The article is concluded in Sec. V.

II. MODEL AND THEORY

Let us start the CSM by considering first the steady-state transport of electrons in the MQWs in the presence of $\mathcal{E}_b(t)$. If $\mathcal{E}_b(t)$ is time independent, the electrons undergo a Fowler–Nordheim tunneling process[4] through the barrier to give rise to a dc current. Here, the charge density (CD) in each QW remains at its equilibrium value n_{2D}. If $\mathcal{E}_b(t)$ be-

comes time dependent, the electrons respond to it by producing an ac current. If $I_a[\mathcal{E}_b(t)]$ at each time depends on $\mathcal{E}_b(t)$ instantaneously, this tunneling process is said to be adiabatic, and will not remember anything that happened earlier. In reality, however, we find that the existence of current hysteresis indicates that tunneling electrons do remember what occurred previously, and thus the tunneling process must be nonadiabatic in nature. In fact, we find that the tunneling current depends not only on $\mathcal{E}_b(t)$, but also on $d\mathcal{E}_b(t)/dt$. In the nonadiabatic tunneling process, the CD in each QW changes with time and fluctuates around n_{2D} when $\mathcal{E}_b(t)$ is applied, which is described well by a nonadiabatic field $\mathcal{E}_{na}(t)$. This field can be either positive or negative when the CD in the QWs is lower or higher than n_{2D}. In the following, we will establish a dynamical equation for $\mathcal{E}_{na}(t)$ within the CSM.

Using Levine's SET current formula,[5] we are led to

$$I_a[\mathcal{E}_b(t)] = e\mathcal{S}v_d[\mathcal{E}_b(t)]n_{\text{eff}}[\mathcal{E}_b(t),T_e], \tag{1}$$

where T_e is the electron temperature and $\mathcal{S}$ is the sample cross-sectional area. The drift velocity $v_d[\mathcal{E}_b(t)]$ in Eq. (1) is related to $\mathcal{E}_b(t)$ by a saturation model,[6] and the effective three-dimensional electron tunneling density $n_{\text{eff}}[\mathcal{E}_b(t),T_e]$ is defined through

$$n_{\text{eff}}[\mathcal{E}_b(t),T_e] = (m^*/\pi\hbar^2 L_W)\int_0^{+\infty} dE\, T[E,\mathcal{E}_b(t)]$$
$$\times\{f_0[E+E_1]-f_0[E+E_1+eL_B\mathcal{E}_b(t)]\}, \tag{2}$$

where $\mu_c(T_e)$ is the chemical potential of electrons in each QW and $f_0(X)=\{1+\exp[X-\mu_c(T_e)/k_B T_e)]\}^{-1}$. $E_1[\mathcal{E}_b(t)]-\mu_c[T_e,\mathcal{E}_b(t)]$ is independent of $\mathcal{E}_b(t)$ and is denoted simply by $E_1-\mu_c(T_e)$. In Eq. (2), m^* is the effective mass of electrons, L_W is the width of each QW, and L_B is the thickness of the barrier between adjacent QWs. E_1 is the ground-state energy of electrons at $\mathcal{E}_b(t)=0$,[7] and $T[E,\mathcal{E}_b(t)]$ is the transmission coefficient of electrons with incident energy E through a biased barrier.[8] Because the SET time is on the order of $\sim 1\ \mu s$, which is much smaller than the variation time of $\mathcal{E}_b(t)$, $T[E,\mathcal{E}_b(t)]$ can be evaluated by using the time-independent Schrödinger equation for each value of $\mathcal{E}_b(t)$.

When $d\mathcal{E}_b(t)/dt \neq 0$ in the nonadiabatic limit, there exists a current surge $I_s(t)$ in addition to $I_a[\mathcal{E}_b(t)]$, which is given by

$$I_s(t) = (m^* e\mathcal{S}/\pi\hbar^2)\lim_{\Delta t\to 0}(1/\Delta t)\int_0^{+\infty} dE\{f_0[E+E_1$$
$$+eL_B\Delta t\, d\mathcal{E}_b(t)/dt]-f_0[E+E_1]\}$$
$$= -f_0[E_1](m^* e^2\mathcal{S}L_B/\pi\hbar^2)d\mathcal{E}_b(t)/dt. \tag{3}$$

When we ignore $I_s(t)$, CDs in different QWs all equal n_{2D}. The existence of $I_s(t)$ drives the CD in each QW away from n_{2D}. The charge fluctuation $\Delta Q(t)$ in the QW induces the $\mathcal{E}_{na}(t)$ in the system, which gives rise to an additional nonadiabatic current

$$I_{na}(t) = e\mathcal{S}\{v_d[\mathcal{E}_b(t)+\mathcal{E}_{na}(t)]n_{\text{eff}}[\mathcal{E}_b(t)+\mathcal{E}_{na}(t),T_e]$$
$$-v_d[\mathcal{E}_b(t)]n_{\text{eff}}[\mathcal{E}_b(t),T_e]\}. \tag{4}$$

In terms of $\mathcal{E}_{na}(t)$, we can calculate $\Delta Q(t)$ in the QW.[9] The quantum-mechanical continuity equation $I_{na}(t)+I_s(t)+d\Delta Q(t)/dt=0$ leads to the following dynamical equation for $\mathcal{E}_{na}(t)$:

$$C_{QW}[\mathcal{E}_{na}(t)]d\mathcal{E}_{na}(t)/dt$$
$$= C_{QW}[0]d\mathcal{E}_b(t)/dt-(e\mathcal{S}/L_B)\{v_d[\mathcal{E}_b(t)$$
$$+\mathcal{E}_{na}(t)]n_{\text{eff}}[\mathcal{E}_b(t)+\mathcal{E}_{na}(t),T_e]$$
$$-v_d[\mathcal{E}_b(t)]n_{\text{eff}}[\mathcal{E}_b(t),T_e]\}, \tag{5}$$

where $C_{QW}[\mathcal{E}_{na}(t)]$ is the QW capacitance.[10] The total tunneling current is $I_a[\mathcal{E}_b(t)]+I_{na}(t)$. If the inequality $|\mathcal{E}_{na}(t)| \ll |\mathcal{E}_b(t)|,\mu_c(T_e)/eL_B$ is satisfied in the limit of slowly varying $\mathcal{E}_b(t)$, we can expand Eq. (5) to the first order in $\mathcal{E}_{na}(t)$. Consequently, Eq. (5) is simplified to

$$d\mathcal{E}_{na}(t)/dt = d\mathcal{E}_b(t)/dt-\mathcal{E}_{na}(t)/\{R_d[\mathcal{E}_b(t)]C_{QW}[0]\}, \tag{6}$$

where $R_d[\mathcal{E}_b(t)]$ is the differential tunneling resistance.[11] Equation (6) is identical to the previously derived circuit equation[1] by rewriting $V_b(t)=L_B\mathcal{E}_b(t)$ and $V_c(t)=V_b(t)-L_B\mathcal{E}_{na}(t)$. Equation (6) can be viewed as the charging /discharging circuit equation with respect to $\mathcal{E}_{na}(t)$ in the presence of a source term $d\mathcal{E}_b(t)/dt$, in which $R_d[\mathcal{E}_b(t)]C_{QW}[0]$ plays the role of MCDT. This uncovers the microscopic origin of the circuit model[1] and explicitly relates the MCDT to the change of microscopic tunneling current in the MQWs.

III. NUMERICAL RESULTS AND DISCUSSIONS

In our calculation, we assign two forms to $\mathcal{E}_b(t)$ as follows:

$$\mathcal{E}_b(t) = \begin{cases} \sum_{j=1}\Delta\mathcal{E}_j\{1/2+1/\pi\,\tan^{-1}[(t-t_j)/\Gamma_j]\} \\ \mathcal{E}_m\sin[2\pi(t+t_0)/T_p]. \end{cases} \tag{7}$$

In Eq. (7), $(t_{j+1}-t_j)$, Γ_j, and $\Delta\mathcal{E}_j$, respectively, denote the delay time, transition time, and height of the jth step in the step-like $\mathcal{E}_b(t)$, while $\mathcal{E}_m$, T_p, and $2\pi t_0/T_p$ represent the amplitude, period, and initial phase in the sinusoidal $\mathcal{E}_b(t)$. The sample we consider is a MQW structure composed of GaAs wells and $Al_{0.3}Ga_{0.7}As$ barriers. The parameters used in the calculation are: $L_W=50$ Å, $L_B=339$ Å, $T_e=40$ K, $\mathcal{E}_s=2$ kV/cm, $v_s=2\times10^6$ cm/s, $n_{2D}=4.1\times10^{11}$ cm^{-2}, and $\mathcal{S}=2.25\pi\times10^{-4}$ cm^{-2}. The other parameters will be given in the text.

Figure 1 displays both the step-like $\mathcal{E}_b(t)$ (dashed curve) and $\mathcal{E}_b(t)+\mathcal{E}_{na}(t)$ from Eqs. (5) (solid curve) and (6) (dash-dotted curve) as a function of time, where the latter determines $I_a[\mathcal{E}_b(t)]+I_{na}(t)$ according to Eqs. (1) and (4). In the calculation, we take $t_j=j\Delta t$ and $\Gamma_j=\Delta t/20$ with $\Delta t=50$ s for $j=1,2,\ldots,10$. Moreover, we choose $\Delta\mathcal{E}_1=\Delta\mathcal{E}_{10}=-20$ kV/cm and $\Delta\mathcal{E}_j=5$ kV/cm with $j=2,3,\ldots,9$. From Eq. (6), we find $\mathcal{E}_{na}(t)$ is either positive or negative whenever $\mathcal{E}_b(t)$ steps up or down, due to the $I_s(t)$ that results. This corre-
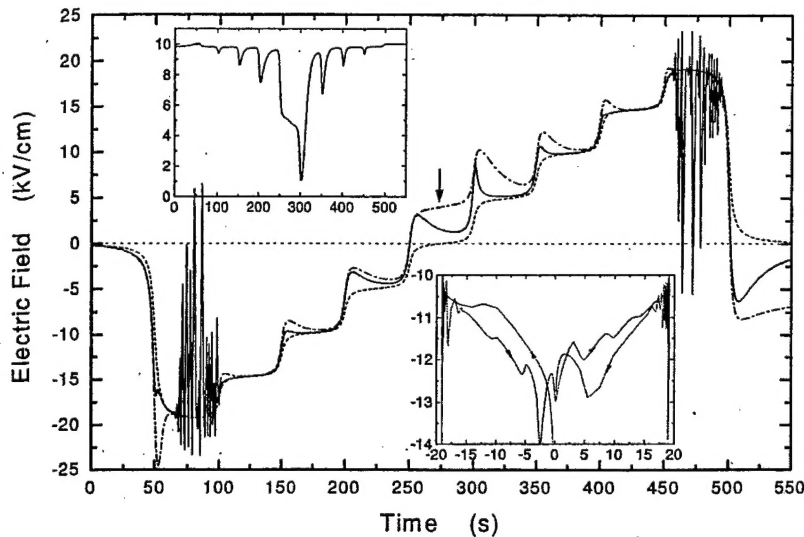
FIG. 1. Step-like $\mathcal{E}_b(t)$ (dashed curve) and $\mathcal{E}_b(t) + \mathcal{E}_{na}(t)$ calculated from Eqs. (5) (solid curve) or (6) (dash-dotted curve) as functions of t, where the dotted line corresponds to zero field and the arrow indicates the time at which $\mathcal{E}_b(t)=0$. The upper inset shows $C_{QW}[\mathcal{E}_{na}(t)]$ (in units of 10^{-10} F) as a function of t (in s), while the lower inset presents $\log\{I_a[\mathcal{E}_b(t)] + I_{na}(t)\}$(current in A) as a function of $\mathcal{E}_b(t)$ (in kV/cm) with arrows indicating how $\mathcal{E}_b(t)$ is varied with t.

sponds to either discharging or charging of electrons. The arrow indicates the time at which $\mathcal{E}_b(t)=0$. The finite $\mathcal{E}_{na}(t)$ at this time is associated with the ZBRTC,[1] as seen in the lower inset. Here, the current ripples due to $I_s(t)$ can be observed each time $\mathcal{E}_b(t)$ jumps. The nonlinear model in Eq. (5) suppresses the effect of $I_s(t)$ by a factor of up to $C_{QW}[0]/C_{QW}[\mathcal{E}_{na}(t)]\sim10^{-1}$, where $C_{QW}[\mathcal{E}_{na}(t)]$ is shown in the upper inset. $C_{QW}[\mathcal{E}_{na}(t)]$ develops a series of peaks at the time when $\mathcal{E}_b(t)$ jumps. The peak strength increases with $R_d[\mathcal{E}_b(t)]$. The current oscillations at ±20 kV/cm seen in the lower inset of Fig. 1 are due to the current bistability. We will describe this bistability and the resulting current instability when we discuss Fig. 2.

In Fig. 2 we present the logarithm of $I_a[\mathcal{E}_b(t)]+I_{na}(t)$, using Eqs. (5) (solid curve) or (6) (dashed curve) as a function the sinusoidal $\mathcal{E}_b(t)$. In the calculation, $t_0=10^{-2}$ s, $T_p =400$ s and $\mathcal{E}_m=18$ kV/cm are chosen. From the figure, we see a current arch supported by $I_a[\mathcal{E}_b(t)]+I_{na}(t)=0$ at the two symmetric finite values of $\mathcal{E}_b(t)$ (the current "offset" of Ref. 1). The nonlinear model tends to squeeze the width of the current arch and increases the ZBRTC. For a sinusoidal

$\mathcal{E}_b(t)$, we again find the current oscillations around ±18 kV/cm due to a bistability in the current. The left inset shows $\mathcal{E}_b(t)$ (dashed curve) and $\mathcal{E}_b(t)+\mathcal{E}_{na}(t)$ from Eqs. (5) (solid curve) and (6) (dash-dotted curve) as a function of time, where the current oscillations are found in $\mathcal{E}_{na}(t)$ around $d\mathcal{E}_b(t)/dt=0$. From it, we further find the deformation of $\mathcal{E}_b(t)+\mathcal{E}_{na}(t)$ relative to $\mathcal{E}_b(t)$, which develops into a phase delay between them when $T_p=40$ s (not seen here). The finite zero-current fields are indicated by the two arrows in the right inset, where the current hysteresis can be clearly seen.

The current instability arising at high electric fields can be explained as follows. A current bistability is found in this system within the nonlinear model which supports the solution with $d\mathcal{E}_{na}(t)/dt=0$ but $\mathcal{E}_{na}(t)\neq0$ around $d\mathcal{E}_b(t)/dt=0$. Due to the current hysteresis as shown in the right inset of Fig. 2, we can always find a pair of bistable points which show the same total tunneling current at $\mathcal{E}_{b1}$ and $\mathcal{E}_{b2}$. The field difference $\delta\mathcal{E}_b=|\mathcal{E}_{b1}-\mathcal{E}_{b2}|$ between the bistable points decreases as $|\mathcal{E}_b(t)|$ increases. From Eq. (5) we know when
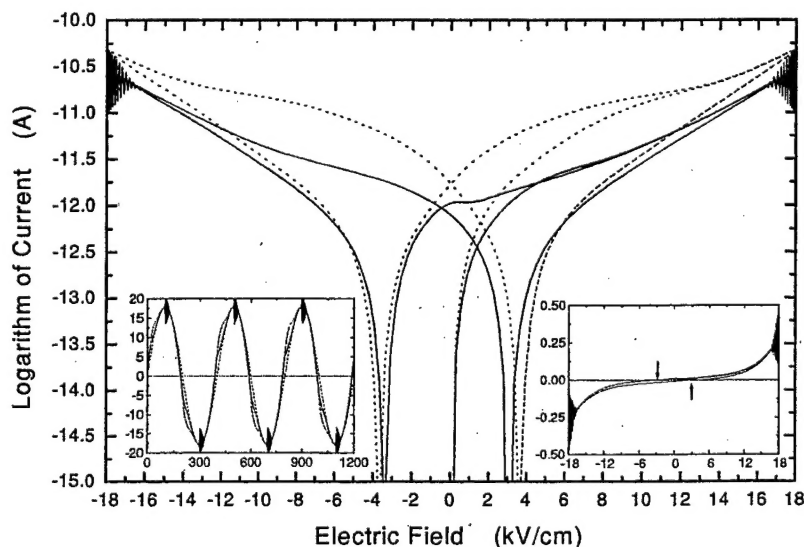

FIG. 2. Results of $\log\{I_a[\mathcal{E}_b(t)]+I_{na}(t)\}$ using Eqs. (5) (solid curve) or (6) (dashed curve) as a function of sinusoidal $\mathcal{E}_b(t)$. The left inset shows $\mathcal{E}_b(t)$ (dashed curve) and $\mathcal{E}_b(t)+\mathcal{E}_{na}(t)$ calculated from Eqs. (5) (solid curve) or (6) (dash-dotted curve) (in kV/cm) as a function of t (in s), where the dotted line represents zero field. The right inset presents the calculated $I_a[\mathcal{E}_b(t)]+I_{na}(t)$ (in units of 10^{-10} A), as a function of $\mathcal{E}_b(t)$ (in kV/cm), where the two arrows indicate the finite zero-current fields.
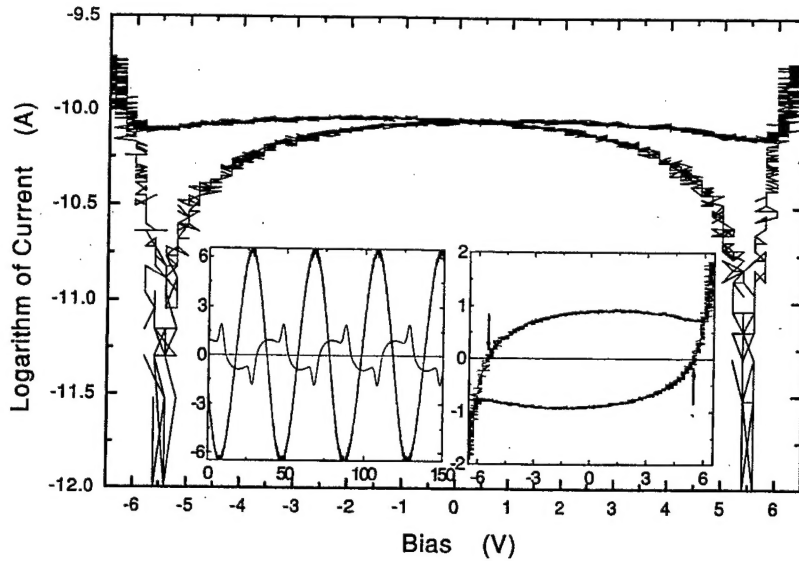
FIG. 3. Experimental data for the logarithm of the tunneling current as a function of the applied sinusoidal bias. The left inset shows the bias (in V), the curve with the large oscillating amplitude, and the measured current (in units of 10^{-10} A), the curve with the small oscillating amplitude, as functions of time (in s), where the dash-dotted line represents the zero current and bias. The right inset presents the measured current (in units of 10^{-10} A) as a function of the bias (in V), where the two arrows indicate the finite zero-current biases.

$d\mathcal{E}_b(t)/dt \approx 0$, $d\mathcal{E}_{na}(t)/dt$ approaches zero if $\delta\mathcal{E}_b = |\mathcal{E}_{na}(t)|$ at a particular time. This causes $d\mathcal{E}_{na}(t)/dt$ to switch its sign before and after this time, leading to an instability of the tunneling current. We further note that the current instability can survive only around $|\mathcal{E}_b(t)| \geqslant 18$ kV/cm where the condition $\delta\mathcal{E}_b \leqslant |\mathcal{E}_{na}(t)|$ can be satisfied and will die away as $\delta\mathcal{E}_b > |\mathcal{E}_b(t)|$ for smaller $|\mathcal{E}_b(t)|$. However, in Eq. (6) the current instability is absent and replaced by a decaying process for $\mathcal{E}_{na}(t)$ which ends with $d\mathcal{E}_{na}(t)/dt = \mathcal{E}_{na}(t) = 0$.

IV. EXPERIMENTAL RESULTS AND COMPARISONS

The experiment was designed to measure the tunneling current in the MQWs under a sinusoidally varying bias with frequency as low as 0.01 Hz. The device was mounted in a Dewar cooled with liquid He, and a darkened metal plate was placed at the aperture of the Dewar. A cold shield was inserted over the device. All these precautions were taken to ensure that we measured the current in the absence of photons. A function generator was used to generate the sinusoidal wave form, and an electrometer with femto-amp resolution was used to measure the current. The electrometer had an analog voltage output which was connected to a digitizing oscilloscope to display the signals with frequencies down to 0.01 Hz. The applied and measured wave forms were observed simultaneously on the oscilloscope.

Figure 3 presents the logarithm of the experimentally measured tunneling current as a function of the applied bias. The sample used in the measurement is a 50 period $Al_{0.3}Ga_{0.7}As$/GaAs MQW structure and its parameters are listed as follows: $L_W = 50$ Å , $L_B = 309$ Å , $T_e = 40$ K, $n_{2D} = 2.5 \times 10^{11}$ cm^{-2}, and $\mathcal{S} = 10^{-4}$ cm^{-2}. We used a sinusoidal bias with $\mathcal{V}_m = 6$ V and $T_p = 40$ s, where $\mathcal{E}_m$ is related to $\mathcal{V}_m$ through $\mathcal{E}_m = \mathcal{V}_m/50(L_B + L_W)$. The pillars of the current arch predicted in Fig. 2 are observed at ± 5.5 V in our measurement. The left inset proves the existence of the current instability, shown as an additional peak superposed on

the shoulder of the sinusoid-like tunneling current with a phase delay with respect to the bias. The right inset confirms the current hysteresis predicted in Fig. 2. The fattened shape of the current hysteresis curve makes it very difficult to observe the current oscillations with more than one period since the field difference between the bistable points is very large. The current ripples seen in Fig. 1 are also observed from our experiment and will be presented elsewhere.

V. CONCLUSIONS

In conclusion, by proposing the CSM, we have explored the mystery of the observation of the microscopic tunneling current change on a macroscopic time scale and found the microscopic origin of the previously reported circuit model used to explain the ZBRTC. The physics of the tunneling process with a very large time constant in the MQWs has been elucidated. With the CSM we have predicted some additional features of the tunneling current in the presence of a time-dependent bias, including a current ripple, current hysteresis, a current arch, and current instability. All of these predictions have been confirmed by our experiment.

[1] A. Singh and D. A. Cardimona Opt. Eng. (Bellingham) 38, 1424 (1999).
[2] U. Meirav, M. A. Kastner, and S. J. Wind, Phys. Lett. 65, 771 (1990).
[3] D. Luis, H. Cruz, and N. E. Capuj, Phys. Rev. B 59, 9787 (1999).
[4] G. M. Williams, R. E. DeWams, C. W. Farley, and R. J. Anderson, Appl. Phys. Lett. 60, 1324 (1992).
[5] B. F. Levine J. Appl. Phys. 74, R1 (1993).
[6] Within the saturation model, we have $v_d[\mathcal{E}_b(t)] = \{v_s / \sqrt{1 + [\mathcal{E}_b(t)/\mathcal{E}_s]^2}\} \times [\mathcal{E}_b(t)/\mathcal{E}_s]$, where v_s is the saturation velocity and $\mathcal{E}_s$ is the saturation field.
[7] D. H. Huang and M. O. Manasreh, J. Appl. Phys. 81, 1305 (1997).
[8] D. Huang, D. A. Cardimona, and A. Singh, Phys. Lett. A 243, 335 (1998).
[9] The charge fluctuation around n_{2D} in each QW is calculated by $\Delta Q(t) = (m^* e \mathcal{S}/\pi\hbar^2) \int_0^{+\infty} dE\{f_0[E+E_1] - f_0[E+E_1+eL_B\mathcal{E}_{na}(t)]\}$.
[10] The QW capacitance is given by $C_{QW}[\mathcal{E}_{na}(t)] = f_0[E_1+eL_B\mathcal{E}_{na}(t)] \times (m^* e^2 \mathcal{S}/\pi\hbar^2)$.
[11] The inverse of differential resistance for SET in the MQWs is $1/R_d[\mathcal{E}_b(t)] = (e\mathcal{S}/L_B)\partial/\partial\mathcal{E}_b\{v_d[\mathcal{E}_b(t)]n_{eff}[\mathcal{E}_b(t),T_e]\}$.